AGU PUBLICATIONS

Geophysical Research Letters

RESEARCH LETTER
10.1002/2016GL070342

Key Points:
- SCS's magnetic property change coincides with global climate transitions
- SCS deep current increased during H1 and the Younger Dryas
- SCS deep current increases due to enhanced NPDW formation

Supporting Information:
- Data Set S1
- Supporting Information S1

Correspondence to:
Z. Chen,
chzhsouth@scsio.ac.cn

Citation:
Zheng, X., et al. (2016), Deepwater circulation variation in the South China Sea since the Last Glacial Maximum, *Geophys. Res. Lett.*, *43*, 8590–8599, doi:10.1002/2016GL070342.

Received 6 JUL 2016
Accepted 29 JUL 2016
Accepted article online 30 JUL 2016
Published online 19 AUG 2016

Deepwater circulation variation in the South China Sea since the Last Glacial Maximum

Xufeng Zheng[1], ShuhJi Kao[2], Zhong Chen[1], Laurie Menviel[3], Han Chen[4], Yan Du[5], Shiming Wan[6], Hong Yan[7], Zhonghui Liu[8], Liwei Zheng[2], Shuhong Wang[1], Dawei Li[2], and Xu Zhang[9]

[1]Key Laboratory of Marginal Sea Geology, South China Sea Institute of Oceanology, Chinese Academy of Sciences, Guangzhou, China, [2]State Key Laboratory of Marine Environmental Science, Xiamen University, Xiamen, China, [3]Climate Change Research Centre, ARC Centre of Excellence for Climate System Science, University of New South Wales, Sydney, Australia, [4]Island Research Center, State Oceanic Administration, Fuzhou, China, [5]State Key Laboratory of Tropical Oceanography, South China Sea Institute of Oceanology, Chinese Academy of Sciences, Guangzhou, China, [6]Key Laboratory of Marine Geology and Environment, Institute of Oceanology, Chinese Academy of Sciences (CAS), Qingdao, China, [7]State Key Laboratory of Loess and Quaternary Geology, Institute of Earth Environment, Chinese Academy of Sciences, Xi'an, China, [8]Department of Earth Sciences, University of Hong Kong, Hong Kong, China, [9]Alfred-Wegener-Institut, Helmholtz-Zentrumfür Polar- und Meeresforschung, Bremerhaven, Germany

Abstract Deepwater circulation plays a central role in global climate. Compared with the Atlantic, the Pacific deepwater circulation's history remains unclear. The Luzon overflow, a branch of the North Pacific deep water, determines the ventilation rate of the South China Sea (SCS) basin. Sedimentary magnetic properties in the SCS reflect millennial-scale fluctuations in deep current intensity and orientation. The data suggest a slightly stronger current at the Last Glacial Maximum compared to the Holocene. But, the most striking increase in deep current occurred during Heinrich stadial 1 (H1) and to a lesser extent during the Younger Dryas (YD). Results of a transient deglacial experiment suggest that the northeastern current strengthening at the entrance of the SCS during H1 and the YD, times of weak North Atlantic Deep Water formation, could be linked to enhanced formation of North Pacific Deep Water.

1. Introduction

Intermediate-deepwater circulation plays a central role in climate change [*Marshall and Speer*, 2012]. Intermediate and deep waters sink to the deep ocean at high latitudes and ultimately return to the surface driving the meridional overturning circulation (MOC) [*Kuhlbrodt et al*., 2007; *McManus et al*., 2004]. Changes in intermediate-deepwater circulation may influence the storage of carbon in the ocean; the oxygen supply; and thus, the extent of the oxygen minimum zones [*Galbraith et al*., 2007] as well as the sediment dispersion and burial [*McCave et al*., 1995]. Understanding changes in intermediate and deepwater currents is crucial to constrain past changes in climates and ocean biogeochemistry.

The last deglaciation was punctuated by millennial climate changes, such as Heinrich event 1 (H1) and the Younger Dryas (YD) [*Blunier and Brook*, 2001; *Dansgaard et al*., 1993], during which North Atlantic Deep Water (NADW) formation weakened significantly [*McManus et al*., 2004]. Modeling studies and paleoproxy records have suggested that a shutdown of NADW formation could lead to enhanced North Pacific Deep Water (NPDW) formation due to atmospheric and oceanic teleconnections [e.g., *Saenko et al*., 2004; *Okumura et al*., 2009; *Okazaki et al*., 2010; *Rae et al*., 2014]. While these paleoreconstructions are derived from high to middle latitudes (close to NPDW formation region), there is a lack of records from lower latitudes. Given its location, close to the NPDW potential path, the South China Sea (SCS) provides a key area to test whether NPDW was significantly stronger during North Atlantic stadials.

The SCS, located in the tropical to subtropical western North Pacific (NP), is the largest marginal sea in the western Pacific. An overflow of North Pacific water through the Luzon Strait connects the SCS and the Pacific Ocean at a depth of about 2400 m (sill depth) and sustains deep circulation in the SCS (Figure 1) [*Qu et al*., 2006]. Similarities in physical and chemical properties between deep water in the SCS basin and the Pacific at 2000 m [*Wang et al*., 2011] suggest that the SCS deep water originates from NPDW. The high sedimentation rates in the SCS and the tight connection between the SCS and the NP make the SCS an ideal location to reconstruct North Pacific intermediate/deep current history and its link to North Atlantic millennial-scale variability.

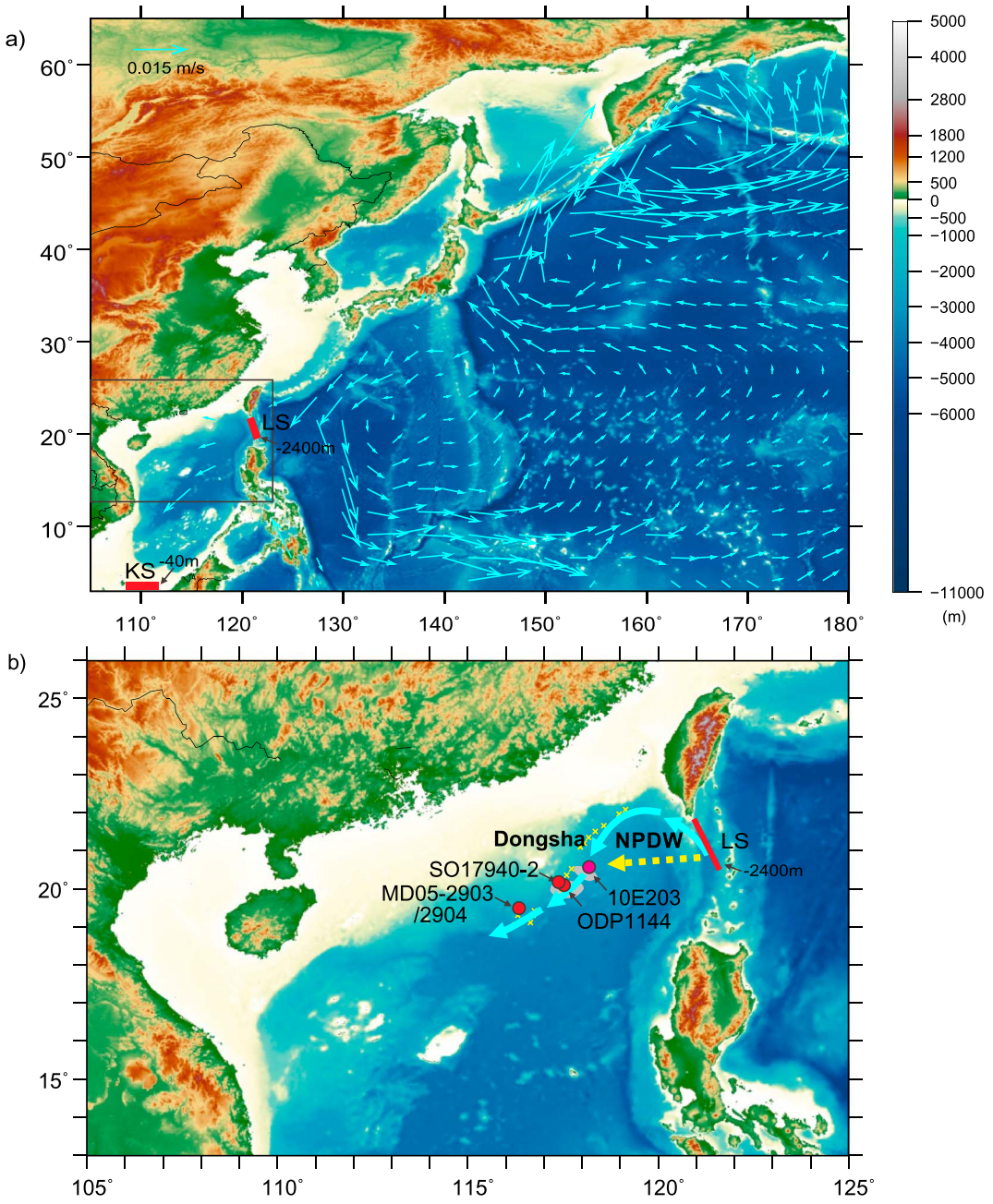

Figure 1. (a) Ocean bathymetry in the North Pacific (color) and ocean currents (m/s) at 1992–2622 m depth at the LGM as simulated in LOVECLIM Earth system model [*Menviel et al.*, 2011]. (b) A schematic map with the enlargement of the black square in Figure 1a to show the topography and current system in the NE part of the SCS, with spatial references of cores locations. NPDW = North Pacific Deep Water. The core 10E203 marked with pink color was the primary core analyzed in this study. The red colored circles are the cores to which we referred. The yellow dashed line is the deep current route proposed by *Lüdman et al.* [2005]. The cyan solid line is the deep current path revealed by *Liu et al.* [2010] and *Shao et al.* [2007]. Sediment drift: yellow crosses [*Shao et al.*, 2007] and grey shaded area [*Lüdman et al.*, 2005]. LS and KS represent the Luzon Strait (−2400 m) and Karimata Strait (−40 m), respectively (red bar).

Observed water properties [*Wang et al.*, 2011] and numerical modeling [*Lan et al.*, 2015] suggest a basin-scale cyclonic gyre path in the SCS below 2400 m water depth, forced by the Luzon overflow. The incoming SCS deep water flows southward and rises in the southern basin, forming the general SCS MOC-like deep circulation system [*Shu et al.*, 2014]. By using seismic profile analyses (drift sediment accretion), *Lüdmann et al.* [2005] suggested that the overflow water possesses enough energy to flow up directly crossing the northern slope

of the SCS basin near Dongsha Island (Figure 1). However, *Shao et al*. [2007], employing a similar method, revealed persistent cyclonic deep circulation along the isobaths since 3 Ma. Temporal and spatial variabilities of clay mineral assemblages in sediments from the northeastern (NE) SCS also support a basin-scale cyclonic gyre pattern of deep circulation [*Liu et al*., 2008, 2010; *Wan et al*., 2010], agreeing with the aforementioned modeling and present-day observations. However, seismic profile and clay mineral distribution methods are qualitative in nature; a more specific method to quantify the current orientation is required to address the debate.

Previous paleoreconstructions from the SCS based on $\delta^{13}C$ and ventilation age changes revealed significant temporal variability in deepwater advection within the SCS since the Last Glacial Maximum (LGM) [*Wan and Jian*, 2014; *Wei et al*., 2006]. However, an additional high-resolution archive is urgently needed to better constrain the deglacial SCS deep water's history, its relationship to deep circulation in the NP and to North Atlantic millennial-scale climatic events.

Magnetic properties, i.e., magnetic grain size proxies and fabric alignment coefficients, are sensitive to bottom current dynamics and are not affected by changes in sedimentation rate [*Kissel et al*., 1997, 2009]. Magnetic properties are routinely used to reconstruct paleoflow's magnitude and azimuth [*Kissel et al*., 2009, 2013]. Based on paleomagnetic parameters of a SCS sediment core, we herein reconstruct the evolutionary history of the SCS deep current since the LGM at a centennial to millennial time scale. The temporal variations of the deep current's intensity support the Atlantic-Pacific interbasin seesaw theory.

2. Materials and Methods

A sediment core (10E203), (118°23.351'E, 20°34.963'N), 3.44 m in length, was collected during the "OPEN AND SHARE" cruise. It is located on the NE slope of the SCS, at a depth of 2439 m (Figure 1). This core lies within the flowing path of the SCS deep cyclonic circulation and, as evidenced by sediment drifts deposition [*Shao et al*., 2007], is situated where the NPDW branch encounters the slope of the SCS basin (Figure 1).

Core lithology is dominated by terrigenous clayed silt with successive laminations. Planktonic foraminifera (*Neogloboquadrina dutertrei*) were isolated from a selection of fine-grained sediment layers for ^{14}C dating (accelerator mass spectrometry (AMS) laboratory, Beta Analytic). The age model is based on 10 AMS ^{14}C ages (Figure S1 in the supporting information). Calendar age is determined by using Calib 7.0 with a regional ^{14}C reservoir age of $\Delta R = 18 \pm 37$ [*Yu et al*., 2010]. Core 10E203 is characterized by a high, yet stable, depositional rate (50 yr/cm; Figure S1). This offers a valuable archive to explore the deep circulation at centennial to millennial time scales.

Paleomagnetic samples were prepared using a standard $2 \times 2 \times 2$ cm plastic cube at 2 to 4 cm intervals (total 100 samples) along a fiducial line that was drawn prior to sampling. Low-field magnetic susceptibility (k), magnitude and the direction of the anisotropy of magnetic susceptibility (AMS), saturated isothermal remanent magnetization (SIRM), anhysteretic remanent magnetization (ARM), and characteristic remanent magnetization (ChRM) analyses were measured according to *Wu et al*. [2016].

The mean ChRM was acquired for each section in order to reorient the core to geographical north according to *Parés et al*. [2007] (see Table S1 in the supporting information). Statistical analyses on the inclination of k_{max} and k_{min} were conducted to infer if core 10E203 was a nonperturbed system after deposition (Figure S2). Volumetric magnetic susceptibility as a function of temperature (k versus T) was measured for six samples from room temperature to 700°C using CS4/CSL high- and low-temperature units attached to the MFK1-FA instrument to infer the main magnetic mineral composition of this sediment core (Figure S2).

Five samples were chosen to conduct replicate measurements (5 times). The precision of ARM, SIRM, and k measurement are better than 0.1%, 1.4%, and 0.1%, respectively. The near-bottom flow speed is inferred from magnetic parameters that are sensitive to bottom current, e.g., ARM/k and ARM/SIRM [*Kissel et al*., 2009, 2010]. The degree of AMS (PJ) and the alignment factor (F_s), independent of sedimentation rate, sediment source, or sediment composition [*Ledbetter and Ellwood*, 1980], are calculated to constrain the flow pattern of the deep current.

Anisotropy degree (PJ) [*Jelinek*, 1981]

$$PJ = \exp\left\{2\times\left[(\eta_1-\eta_m)^2+(\eta_2-\eta_m)^2+(\eta_3-\eta_m)^2\right]\right\}^{1/2}$$

Alignment factor (F_s) [*Ellwood*, 1980]

$$F_s = k_{max}{}^2 / \left(k_{int}{}^2 \times k_{min}{}^2\right)^{1/2}$$

where η_1, η_2, and η_3 represent the logarithmic values of k_{max}, k_{int}, and k_{min}, respectively; $\eta_m = (\eta_1 + \eta_2 + \eta_3)/3$.

The deep circulation's paleoflow direction is determined by preferential alignment of the elongated magnetic particles during deposition based on statistical analyses of the azimuth of the k_{max} axes calibrated with mean ChRM (Table S1). This method is more quantitative and efficient than traditional work-intensive optical measurements of the orientation of the grains [*Wolff et al*., 1989]. The preferential orientation of magnetic grains could be affected by several factors, e.g., Earth's gravity field, bottom current, and geomagnetic field [*Hrouda*, 1982]. The Earth's gravity field tends to cause the mineral particles to be deposited with their larger surfaces paralleling to the depositional surface [*Hrouda*, 1982]. The bottom current, however, orients the longer axes of grains parallel to the flow line. Although the geomagnetic field could orient the longer axes of the ferromagnetic grains to the local magnetic meridian, its effect is mainly on fine grains that are not easily deposited when the bottom current is relatively strong. The deposited magnetic grains, thus, record the intensity and orientation of the current rather than the geomagnetic field. This multiproxy paleomagnetic analysis allows us to elucidate the deglacial history of the SCS deep circulation.

3. Results

The k_{min}, k_{int}, and k_{max} represent the minimum, intermediate, and maximum axes of magnetic susceptibility, respectively (Figure S2). k_{min} clusters to the center of the coordinate, while k_{int} and k_{max} are distributed around the edge of the coordinate (Figure S2). The whole-sample susceptibility represents the combined contribution of all magnetite grains, each acting as an individual susceptibility ellipsoid. AMS axis distribution of sample reflects the depositional plane in sediments. Thus, the plane containing k_{max} and k_{int} axes is typically parallel to the depositional surface and the magnetic lineation (cluster of k_{max} axes) is parallel to the paleocurrent direction. A rose diagram of the calibrated declination of k_{max} exhibits that the main azimuths of k_{max} are 65°, 200°, and 243° (Figure S2), which agree with the dominant directions of the deep subinertial current (250° and 70°) observed at the mooring TJ-A-1 at a water depth of 2069 m [*Zhao et al*., 2015]. The inclination of k_{min} ranges from 75° to 90° and k_{max} ranges from 0° to 10° (Figure S2), which are typical index values of a nonperturbed system after deposition [*Kissel et al*., 1997; *Park et al*., 2000]. An inclination of 0~5° accounts for 76%, 5~10° for 18%, 10~15° for 3.5%, and 15~20° for 1.8% in k_{max} (Figure S2). An inclination of 85~90° accounts for 45%, 80~85° for 34%, 75~80° for 15%, 70~75° for 4%, and 65~70° for 1.8% in k_{min} (Figure S2).

Thermomagnetic analyses on bulk samples at six depths reveal a complete loss of magnetization when heated to approximately 580–600°C, which is consistent with the magnetite Curie temperature (Figure S2). Upon cooling, a major increase of magnetization occurs between 580 and 400°C, indicating the possibility of a magnetite production phase during heating (Figure S2).

As magnetite is the dominant magnetic mineral in the sediment, the ARM/*k* and ARM/SIRM ratio, independent of concentration, allow the estimation of magnetite size and thus can be used to trace the SCS deep current's amplitude, with small ARM/*k* and ARM/SIRM indicative of a strong current [*de Menocal et al*., 1988]. The ARM/*k* varies between 0.59 and 1.91 and ARM/SIRM between 0.05×10^{-2} and 1.6×10^{-2}. The variation of ARM/SIRM is largely consistent with that of ARM/*k*. The mean ARM/*k* is slightly lower during the LGM (~1.0) than the middle to late Holocene (MLH, ~1.6); however, the ARM/SIRM is similar for both periods (Figure 2). This implies a similar or slightly stronger deep current at the LGM than during the MLH. Both ARM/*k* and ARM/SIRM display lowest values between 19 and 16 ka, thus indicating a strong deep current during Heinrich stadial 1. Interestingly, another decrease in ARM/*k* and ARM/SIRM, albeit of lower amplitude, is recorded during the Younger Dryas. ARM/*k* and ARM/SIRM are maximum during the early Holocene and gradually decrease toward the middle and late Holocene (MLH) interval.

The magnetic fabric reflects the preferential alignment of the sediment particles during deposition. The downcore PJ and F_s values of core 10E203 document the alignment pattern of the magnetic fabric driven by the deep current through time, with high PJ and F_s values for a good alignment pattern [*Ellwood and Ledbetter*, 1979; *Hamilton and Rees*, 1970]. PJ varies between 1.002 and 1.671 and decreases toward the present. There are three periods with relatively stable values, i.e., 20–17.5, 15–13, and 9–0 ka (Figure 2).

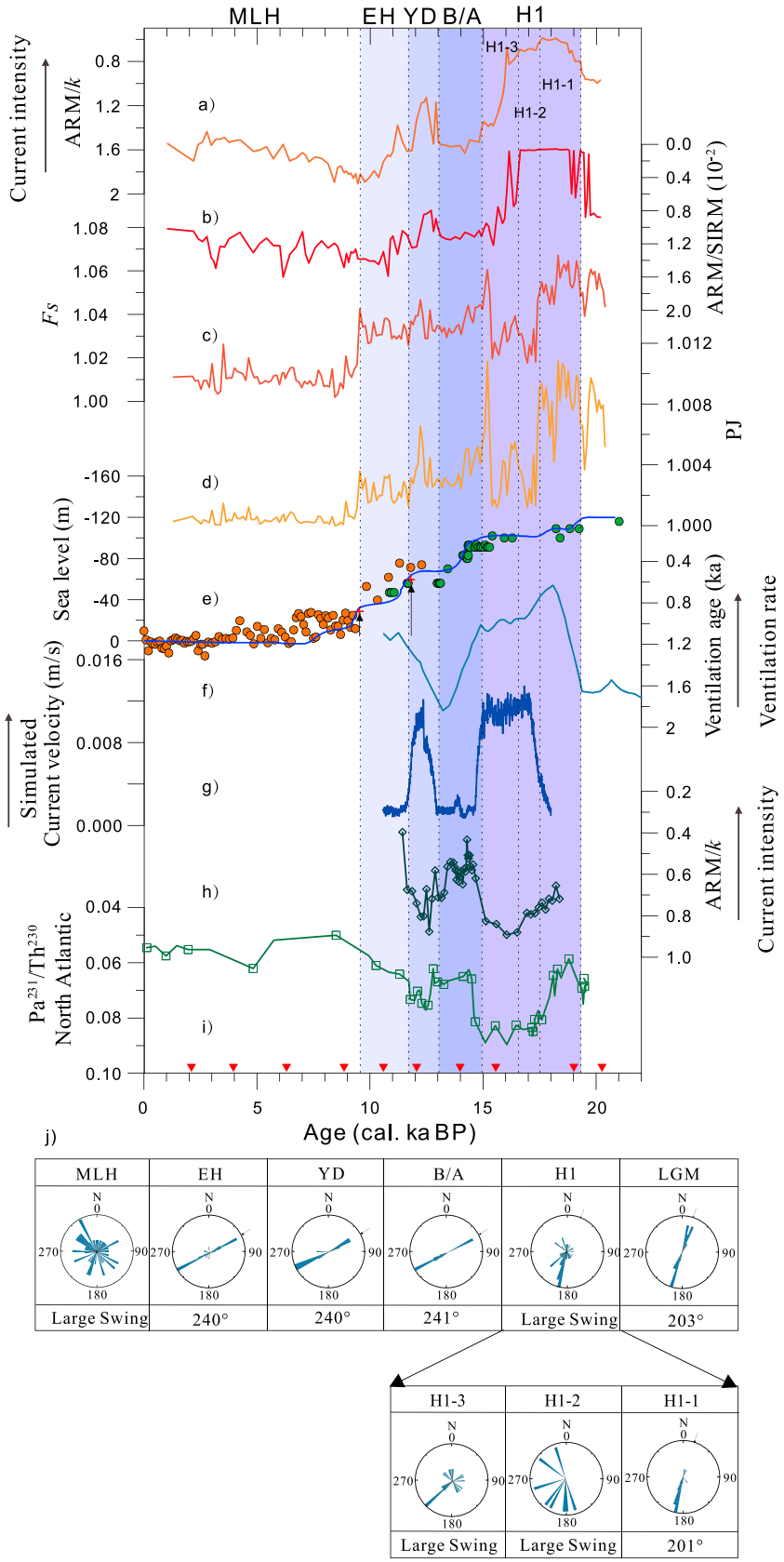
MLH
EH YD B/A
H1
H1-3
H1-1
H1-2
a)
b)
c)
d)
e)
f)
g)
h)
i)
j)
Current intensity
ARM/k
Fs
ARM/SIRM (10-2)
PJ
Sea level (m)
Ventilation age (ka)
Ventilation rate
Simulated Current velocity (m/s)
Pa231/Th230 North Atlantic
Age (cal. ka BP)
MLH
EH
YD
B/A
H1
LGM
Large Swing
240°
240°
241°
Large Swing
203°
H1-3
H1-2
H1-1
Large Swing
Large Swing
201°

Figure 2

Four peaks could also be found at 15, 12.3, 9.2, and 2.9 ka. The temporal variation of F_s is in accordance with PJ, but F_s is less variable during the Holocene interval (Figure 2).

According to well-known climate states, the entire sediment core can be classified into six main intervals, i.e., LGM (20–19 ka), H1 (19–15.1 ka), Bølling/Allerød (B/A) (15.1–13 ka), YD (13–11.6 ka), early Holocene (EH; 11.6–10 ka), and MLH (10–0 ka) [*Stanford et al*., 2011] (Figure 2). The interval of H1 can be further subdivided into three phases, i.e., H1-1, H1-2, and H1-3 based on the temporal variations of the ARM/*k*, ARM/SIRM, PJ, and F_s values (Figure 2). Figure 3a displays the relationship between ARM/*k* and PJ, which indicates the relationship between the current speed and alignment pattern of the magnetic fabric and provides insight into the deep current variability. A clear positive correlation ($R^2 = 0.9029$) between the current speed and alignment pattern of the magnetic fabric was observed except during the H1-2 interval.

During the LGM (20–19 ka), low ARM/*k* and stable k_{max} values (Figure 2) suggest high current velocity and a stable current orientation. A high PJ value also suggests the optimum alignment pattern of the magnetic fabric and indicates a stable current pattern (Figure 3a). The deep current flows along the 2300–2400 m isobath in the NE SCS and shows preferential direction of 201° and 10° (Figures 1 and 2). This implies currents from NE, which is in general agreement with the NE-SW direction of the deep current in SCS, as inferred from the WSW migrating channels and NE prograding drifts in the northern SCS [*Chen et al*., 2014; *Li et al*., 2013]. The SW current could be attributed to seasonal effect imprint as seen from results of subsurface mooring TJ-A-1 [*Zhao et al*., 2015].

During the Last Glacial Termination (19–10 ka), larger variation in ARM/*k*, PJ, and k_{max} values suggest that rapid and large oscillations in current speed and current orientation occurred in concert with global climatic events (Figures 2 and 3a). The most striking transition in the current pattern is observed during H1 (19–15 ka) when sea level was around −100 m. During H1-1 (19–17.5 ka), the deep current speed increased considerably with a stable direction toward the SW (201°), as revealed by the lowest ARM/*k*, stable k_{max}, and large PJ values (Figures 2 and 3a). At the beginning of H1-2 (17.5–16.6 ka), the current direction began fluctuating even though the current speed was persistently strong. An abrupt decrease in PJ suggests a large swing of the deep current (Figure 2). This current direction variability could be ascribed to the divergence of deep currents when strong Luzon overflow intruded into the slope of the northeastern SCS or to diverse streams of current from North Pacific region during the H1-2. Meanwhile, the ARM/*k*-PJ plot indicates a departure from the negative correlation during H1-2 (Figure 3a). This might suggest that the current speed during the H1-2 was too high to maintain the stability of the magnetic fabric, as was observed in the Vema Channel [*Ellwood and Ledbetter*, 1979]. During H1-3 (16.6–15.1 ka), larger error bars in ARM/*k*-PJ plot suggest that both current speed and direction became increasingly unsteady (Figures 2 and 3a), but the current orientation was mainly from NE. Apparently, H1-3's current held large fluctuations in both orientation and intensity, although it followed the negative correlation between the PJ and ARM/*k*.

4. Discussion

During Heinrich event 1, a catastrophic iceberg discharge into the North Atlantic occurred and resulted in a decrease and even cessation of the Atlantic meridional overturning circulation (AMOC) [*Gherardi et al*., 2005; *McManus et al*., 2004]. Recent progress provides a new concept for the evolution of H1 involving the succession of three phases, i.e., the onset of AMOC collapse (19–17.5 ka), the intense Ice Rafted Debris deposition and freshening event (17.5–16.7 ka), and the AMOC resumption period (16.7–15 ka), as revealed by ARM/*k* value of core TTR-451 in Eirik Drift and Pa^{231}/Th^{230} value of core OCE326-GGC5 in Bermuda rise (Figure 2)

Figure 2. Comparison of temporal variations in (a) ARM/*k*, (b) ARM/SIRM, (c) F_s, and (d) PJ of core 10E203. (e) The blue line marks the western Pacific sea level curve [*Liu et al*., 2004], the green circles represent the sea level record from the Sunda shelf [*Hanebuth et al*., 2000], and the orange circles show the sea level record from Red Sea [*Siddall et al*., 2003]. (f) A compiled data set of ventilation age changes in the western North Pacific as previously revealed by *Okazaki et al*. [2010]. (g) Current velocity (m/s) averaged over 122°E–128°E, 18°N–22°N and 1992–2622 m depth as simulated in a transient experiment of the last deglaciation performed with the Earth system model LOVECLIM [*Menviel et al*., 2011]. The Atlantic meridional overturning circulation variability as revealed by (h) ARM/*k* [*Stanford et al*., 2011] and (i) Pa^{231}/Th^{230} in Bermuda rise [*McManus et al*., 2004]. (j) Flow orientation at different intervals as revealed by the azimuth of k_{max}; the red inverted triangles represent the ^{14}C dating points in core 10E203. LGM, H1-1, H1-2, H1-3, B/A, YD, EH, and MLH indicate the different stages of variability of the deep current, respectively.

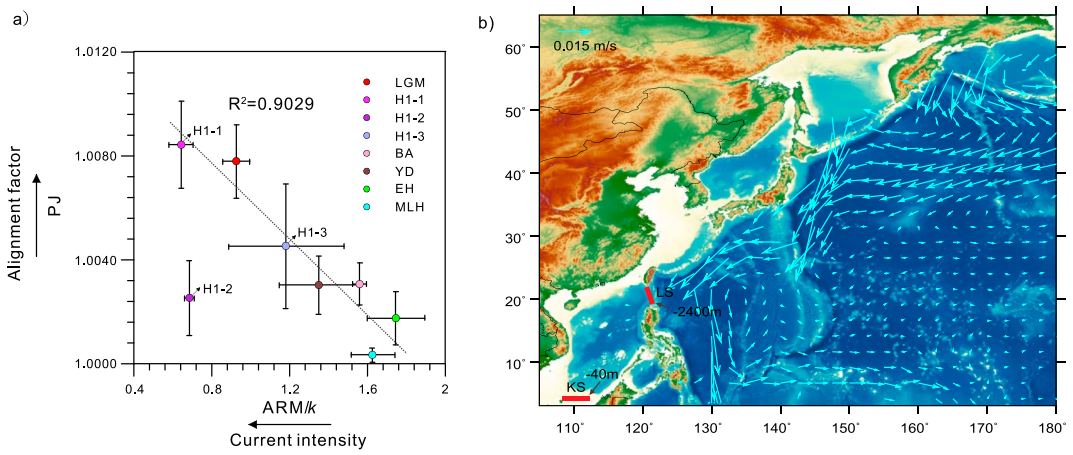

Figure 3. (a) ARM/*k* against PJ plot for LGM, H1-1, H1-2, H1-3, B/A, YD, EH, and MLH intervals (average, standard deviation). (b) Ocean current anomalies (m/s) at 1992–2622 m depth during H1 stadial as simulated in LOVECLIM Earth system model [*Menviel et al*., 2011].

[*McManus et al*., 2004; *Stanford et al*., 2011]. Thus, the three-phase fluctuation in the SCS deep current pattern during H1 could result from a major reorganization of Pacific deep circulation probably linked to AMOC changes [*Menviel et al*., 2011, 2014; *Okumura et al*., 2009; *Saenko et al*., 2004; *Wan and Jian*, 2014].

Radiocarbon records and numerical simulations suggest that NPDW formation was enhanced and extended to a depth of ~2500–3000 m during H1, in response to reduced moisture transport from the Atlantic to Pacific and increased transport of saline low-latitude waters to the North Pacific (Figures 2f and 2g) [*Menviel et al*., 2011; *Okazaki et al*., 2010]. This deep water is analogous to the one currently occurring in the North Atlantic, flowing along the western margin of the North Pacific and penetrating the SCS via the Luzon Strait (Figure 3b) [*Okazaki et al*., 2010; *Wan and Jian*, 2014].

A few paleoproxy records from the upper 2000 m of the North Pacific suggest increased ventilation during H1 compared to the LGM [*Okazaki et al*., 2010; *Jaccard and Galbraith*, 2013; *Max et al*., 2014], while some North Pacific records from water depths greater than 2100 m show little signs of increased ventilation during that time [*Lund et al*., 2011; *Jaccard and Galbraith*, 2013; *Max et al*., 2014]. However, MD02-2489, in the Gulf of Alaska, displays high ventilation rate at 3600 m water depth during H1 [*Rae et al*., 2014], consistent with our paleomagnetic proxies. Nd isotope and ventilation age evidences in cores MD05-2903/2904 and SO17940-2 from the NE SCS also confirm the penetration of deep water into the SCS during the early deglaciation period [*Wan and Jian*, 2014; *Wu et al*., 2015]. The rapid deep current strengthening occurring during H1 in the SCS could thus be associated with the abrupt increase in NPDW on the premise of the terminology of *Talley et al*. [2003] that refers the deep Pacific as water depth >2000 m.

This is in global agreement with a transient deglacial experiment, performed with the Earth system model (LOch–Vecode-Ecbilt-CLio-agIsm Model, LOVECLIM) [*Menviel et al*., 2011], which suggests enhanced NPDW formation during H1 as a result of the AMOC shutdown (Figure 2g). This simulation clearly shows an increase in NE current along the western margin of the North Pacific between ~1443 and 3300 m water depth, with a maximum increase at about 2300 m depth (Figure 3b). However, due to the relatively coarse resolution of the model, the Luzon Strait is at ~1992 m water depth. Thus, a strengthening of the cyclonic circulation in the SCS in response to the stronger NPDW is simulated at 1443–1992 m water depth (Figure S4).

Changes in SCS magnetic properties seem to lead North Atlantic changes by approximately 1000 years during H1 (Figure 2). The weaker summer East Asian monsoon at the LGM compared to the Holocene [*Jiang and Lang*, 2010] could have reduced the North Pacific halocline, thus making it more sensitive to climatic changes. A small AMOC weakening between 19 and 18 ka could have enhanced NPDW formation, which would then strengthen through the Stommel feedback [*Menviel et al*., 2012; *Stommel*, 1961]. This time leading could also be due to a reservoir effect discrepancy in the ^{14}C age model [*Sun et al*., 2005]. Additional studies are needed to validate this lag and address its potential mechanism.

During the B/A (15.1–13 ka), the current velocity weakened and the current direction was restored to a stable condition with an azimuth of around 240° and 60°, concurrently with a strong NADW as shown by ARM/*k* value of core TTR-451 in Eirik Drift and Pa^{231}/Th^{230} value of core OCE326-GGC5 in Bermuda rise (Figures 2 and 3a). The transition of current orientation from 200°, 10° to 240°, 60°occurring from early H1 to B/A further suggests a rapid alternation of the deep current in the SCS.

A subtle reviving of current strength occurred during the YD, as revealed by the ARM/*k* and ARM/SIRM plots (Figures 2 and 3a).

A pulse of intensification in the deep current occurred during the EH (11.6–10 ka), as seen in the ARM/*k* and ARM/SIRM values (Figures 2 and 3a). During this period, sea level was rising up to −40 m, a critical height to reopen the Karimata Strait (KS) to the shallow current throughflow (depth of 40 m) [*Hanebuth et al*., 2000; *Liu et al*., 2004; *Siddall et al*., 2003]. Such topographic changes could increase the replenishing rate of the deep water and thus reduce the water mass resident time (from around 23 to 19 years) in the SCS (Kao et al., under review in Climate of the Past). According to *Qu et al*. [2006], the SCS throughflow (SCSTF) with annual mean value of 3.8 sverdrup involves inflow through the Luzon Strait and outflow mainly through the KS and Mindoro Strait [*Qu et al*., 2006, 2009]. Thus, we speculate that the closure of the KS at low sea level stand might hamper the deep inflow through the Luzon Strait. In contrast, the opening of the KS, connecting the SCS and Indonesia Seas during EH [*Linsley et al*., 2010; *Pelejero et al*., 1999], would increase the outflow of SCS water and naturally increase the Luzon deep inflow. Analyses from cores MD98-2178 and MD98-2161 in the northwestern Celebes Sea also revealed a strengthened SCSTF during the EH, thus corroborating our inference [*Fan et al*., 2013]. However, this pulse of intensification should be investigated further due to the relatively low ARM/k and ARM/SIRM resolution during this interval.

A gradual strengthening of the deep current occurred during the MLH (10–0 ka), although its strength was low when the AMOC was relatively stable (Figures 2 and 3a). The current direction during this period was unsteady (Figure 2). The low PJ values further suggest a slow and variable deep current during the MLH. The ARM/k and ARM/SIRM ratios of site ODP1144 generally agree with our core during the Holocene, thus also supporting the existence of a basin-wide current control (Figures 1 and S3) [*Hu et al*., 2012]. However, all data from ODP1144 prior to 12 ka cannot be used for magnetic susceptibility studies due to diagenetic pyrite formation (Figure S3) [*Hu et al*., 2012].

Until ~12 ka B.P., the SCS deep current intensity was in antiphase with the AMOC intensity (Figures 2h and 2i) [*McManus et al*., 2004; *Stanford et al*., 2011], thus supporting the Atlantic-Pacific interbasin seesaw theory [*Okazaki et al*., 2010]. This is not the case during the Holocene, where changes in SCS deepwater current are not linked to AMOC changes (Figure 2). This could be due to the opening of the Bering Strait at the end of the Younger Dryas. Indeed, with an open Bering Strait, a meltwater-induced AMOC weakening would also freshen the surface waters of the North Pacific, thus preventing NPDW formation. This could also be due to the relatively large influence of the opening of KS on the SCS deepwater characteristics compared to the climatic changes occurring during the Holocene.

Finally, we find that throughout the deglaciation the current directions at core 10E203 were never purely meridional, in contrast to the deep current meridional path previously proposed by *Lüdmann et al*. [2005].

5. Conclusion

Based on magnetic properties of a sediment core taken from the NE SCS, we reconstruct the history of the SCS deep current. We find a slightly stronger deep current at the LGM than during the late Holocene. But, the most striking feature of our record is a significant strengthening of the NE current during Heinrich stadial 1. We suggest that this stronger NE current at about 2300–2400 m water depth in the north SCS during H1 is due to enhanced formation of NPDW and subsequent stronger NE current along the western margin of the North Pacific. The data also suggest slightly stronger deep current in the SCS during the YD. This is supported by a transient experiment of the last deglaciation performed with an Earth system model, showing that a shutdown of the AMOC during H1 and the YD can enhance NPDW formation through oceanic and atmospheric teleconnections [*Menviel et al*., 2011]. We also suggest that the opening of the KS due to sea level rise in the early Holocene likely enhanced deep circulation in the SCS. The overall current intensity variations during the deglaciation were in antiphase with AMOC changes, thus underscoring the tight connection between the Atlantic and Pacific Oceans as well as the interbasin seesaw theory.

Acknowledgments
We are grateful to Catherine Kissel, Xiaodong Tan, Tatiana Ilyina, Naomi Harada, and three anonymous reviewers for providing the insightful suggestions on our manuscript. We thank the crew of the R/V *Shiyan* 3 of South China Sea Institute of Oceanology, Chinese Academy of Sciences, who helped us a lot during the cruise. Our work is supported by the National Natural Science Foundation of China (41506051, 91128206, 41376057, 91328207, and 41430965); the Strategic Priority Research Program of the Chinese Academy of Sciences (XDA11030302); the Guangdong Natural Science Foundation (KLMMR-2015-B-07); and the Key Laboratory of Marine Geology and Environment, Institute of Oceanology, CAS (MGE2015KG03). L. Menviel acknowledges funding from the Australian Research Council grant DE150100107. The data presented in this paper can be found in the supporting information. Our measurement was conducted at Guangzhou Institute of Geochemistry, Chinese Academy of Sciences.

References

Blunier, T., and E. J. Brook (2001), Timing of millennial-scale climate change in Antarctica and Greenland during the Last Glacial Period, *Science*, *291*(5501), 109–112, doi:10.1126/science.291.5501.109.

Chen, H., X. Xie, D. Van Rooij, T. Vandorpe, M. Su, and D. Wang (2014), Depositional characteristics and processes of alongslope currents related to a seamount on the northwestern margin of the Northwest Sub-Basin, South China Sea, *Mar. Geol.*, *355*, 36–53, doi:10.1016/j.margeo.2014.05.008.

Dansgaard, W., S. Johnsen, H. Clausen, D. Dahl-Jensen, N. Gundestrup, C. Hammer, C. Hvidberg, J. Steffensen, A. Sveinbjörnsdottir, and J. Jouzel (1993), Evidence for general instability of past climate from a 250-kyr ice-core record, *Nature*, *364*(6434), 218–220, doi:10.1038/364218a0.

de Menocal, P. B., E. P. Laine, and P. F. Ciesielski (1988), A magnetic signature of bottom current erosion, *Phys. Earth Planet. In.*, *51*(4), 326–348, doi:10.1016/0031-9201(88)90074-X.

Ellwood, B. B. (1980), Application of the anisotropy of magnetic susceptibility method as an indicator of bottom-water flow direction, *Mar. Geol.*, *34*(3), M83–M90, doi:10.1016/0025-3227(80)90066-3.

Ellwood, B. B., and M. T. Ledbetter (1979), Paleocurrent indicators in deep-sea sediment, *Science*, *203*(4387), 1335–1337, doi:10.1126/science.203.4387.1335.

Fan, W., Z. Jian, F. Bassinot, and Z. Chu (2013), Holocene centennial-scale changes of the Indonesian and South China Sea throughflows: Evidences from the Makassar Strait, *Global Planet. Change*, *111*, 111–117, doi:10.1016/j.gloplacha.2013.08.017.

Galbraith, E. D., S. L. Jaccard, T. F. Pedersen, D. M. Sigman, G. H. Haug, M. Cook, J. R. Southon, and R. Francois (2007), Carbon dioxide release from the North Pacific abyss during the last deglaciation, *Nature*, *449*, 890–893, doi:10.1038/nature06227.

Gherardi, J.-M., L. Labeyrie, J. McManus, R. Francois, L. Skinner, and E. Cortijo (2005), Evidence from the Northeastern Atlantic basin for variability in the rate of the meridional overturning circulation through the last deglaciation, *Earth Planet. Sci. Lett.*, *240*, 710–723, doi:10.1016/j.epsl.2005.09.061.

Hamilton, N., and A. Rees (1970), The use of magnetic fabric in paleocurrent estimation, *Palaeogeophysics*, *445*.

Hanebuth, T., K. Stattegger, and P. M. Grootes (2000), Rapid flooding of the Sunda Shelf: A late-glacial sea-level record, *Science*, *288*(5468), 1033–1035, doi:10.1126/science.288.5468.1033.

Hrouda, F. (1982), Magnetic anisotropy of rocks and its application in geology and geophysics, *Geophys. Surv.*, *5*(1), 37–82, doi:10.1007/BF01450244.

Hu, D., P. Böning, C. M. Köhler, S. Hillier, N. Pressling, S. Wan, H. J. Brumsack, and P. D. Clift (2012), Deep sea records of the continental weathering and erosion response to East Asian monsoon intensification since 14 ka in the South China Sea, *Chem. Geol.*, *326–327*, 1–18, doi:10.1016/j.chemgeo.2012.07.024.

Jaccard, S., and E. Galbraith (2013), Direct ventilation of the North Pacific did not reach the deep ocean during the last deglaciation, *Geophys. Res. Lett.*, *40*, 199–203, doi:10.1029/2012GL054118.

Jiang, D., and X. Lang (2010), Last Glacial Maximum East Asian monsoon: Results of PMIP simulations, *J. Clim.*, *23*, 5030–5038, doi:10.1175/2010JCLI3526.1.

Jelinek, V. (1981), Characterization of the magnetic fabric of rocks, *Tectonophysics*, *79*(3), T63–T67, doi:10.1016/0040-1951(81)90110-4.

Kissel, C., C. Laj, B. Lehman, L. Labyrie, and V. Bout-Roumazeilles (1997), Changes in the strength of the Iceland–Scotland Overflow Water in the last 200,000 years: Evidence from magnetic anisotropy analysis of core SU90-33, *Earth Planet. Sci. Lett.*, *152*(1), 25–36, doi:10.1016/S0012-821X(97)00146-5.

Kissel, C., C. Laj, T. Mulder, C. Wandres, and M. Cremer (2009), The magnetic fraction: A tracer of deep water circulation in the North Atlantic, *Earth Planet. Sci. Lett.*, *288*, 444–454, doi:10.1016/j.epsl.2009.10.005.

Kissel, C., C. Laj, M. Kienast, T. Bolliet, A. Holbourn, P. Hill, W. Kuhnt, and P. Braconnot (2010), Monsoon variability and deep oceanic circulation in the western equatorial Pacific over the last climatic cycle: Insights from sedimentary magnetic properties and sortable silt, *Paleoceanography*, *25*, doi:10.1029/2010PA001980.

Kissel, C., A. Van Toer, C. Laj, E. Cortijo, and E. Michel (2013), Variations in the strength of the North Atlantic bottom water during Holocene, *Earth Planet. Sci. Lett.*, *369*, 248–259, doi:10.1016/j.epsl.2013.03.042.

Kuhlbrodt, T., A. Griesel, M. Montoya, A. Levermann, M. Hofmann, and S. Rahmstorf (2007), On the driving processes of the Atlantic meridional overturning circulation, *Rev. Geophys.*, *45*, doi:10.1029/2004RG000166.

Lüdmann, T., H. K. Wong, and K. Berglar (2005), Upward flow of North Pacific Deep Water in the northern South China Sea as deduced from the occurrence of drift sediments, *Geophys. Res. Lett.*, *32*, doi:10.1029/2004GL021967.

Lan, J., Y. Wang, F. Cui, and N. Zhang (2015), Seasonal variation in the South China Sea deep circulation, *J. Geophys. Res. Oceans*, doi:10.1002/2014JC010413.

Ledbetter, M. T., and B. B. Ellwood (1980), Spatial and temporal changes in bottom-water velocity and direction from analysis of particle size and alignment in deep-sea sediment, *Mar. Geol.*, *38*, 245–261, doi:10.1016/0025-3227(80)90062-6.

Li, H., Y. Wang, W. Zhu, Q. Xu, Y. He, W. Tang, H. Zhuo, D. Wang, J. Wu, and D. Li (2013), Seismic characteristics and processes of the Plio-Quaternary unidirectionally migrating channels and contourites in the northern slope of the South China Sea, *Mar. Petrol. Geol.*, *43*, 370–380, doi:10.1016/j.marpetgeo.2012.12.010.

Linsley, B. K., Y. Rosenthal, and D. W. Oppo (2010), Holocene evolution of the Indonesian throughflow and the western Pacific warm pool, *Nat. Geosci.*, *3*, 578–583, doi:10.1038/ngeo920.

Liu, J. P., J. D. Milliman, S. Gao, and P. Cheng (2004), Holocene development of the Yellow River's subaqueous delta, North Yellow Sea, *Mar. Geol.*, *209*, 45–67, doi:10.1016/j.margeo.2004.06.009.

Liu, Z., S. Tuo, C. Colin, J. T. Liu, C.-Y. Huang, K. Selvaraj, C.-T. A. Chen, Y. Zhao, F. P. Siringan, and S. Boulay (2008), Detrital fine-grained sediment contribution from Taiwan to the northern South China Sea and its relation to regional ocean circulation, *Mar. Geol.*, *255*, 149–155, doi:10.1016/j.margeo.2008.08.003.

Liu, Z., C. Colin, X. Li, Y. Zhao, S. Tuo, Z. Chen, F. P. Siringan, J. T. Liu, C.-Y. Huang, and C.-F. You (2010), Clay mineral distribution in surface sediments of the northeastern South China Sea and surrounding fluvial drainage basins: Source and transport, *Mar. Geol.*, *277*, 48–60, doi:10.1016/j.margeo.2010.08.010.

Lund, D. C., A. C. Mix, and J. Southon (2011), Increased ventilation age of the deep northeast Pacific Ocean during the last deglaciation, *Nat. Geosci.*, *4*, 771–774, doi:10.1038/ngeo1272.

Marshall, J., and K. Speer (2012), Closure of the meridional overturning circulation through Southern Ocean upwelling, *Nat. Geosci.*, *5*, 171–180, doi:10.1038/ngeo1391.

Max, L., L. Lembke-Jene, J.-R. Riethdorf, R. Tiedemann, D. Nürnberg, H. Kühn, and A. Mackensen (2014), Pulses of enhanced North Pacific Intermediate Water ventilation from the Okhotsk Sea and Bering Sea during the last deglaciation, *Clim. Past*, *10*, 591–605, doi:10.5194/cp-10-591-2014.

McCave, I. N., B. Manighetti, and S. G. Robinson (1995), Sortable silt and fine sediment size/composition slicing: Parameters for palaeocurrent speed and palaeoceanography, *Paleoceanography*, *10*(3), 593–610, doi:10.1029/94PA03039.

McManus, J., R. Francois, J.-M. Gherardi, L. Keigwin, and S. Brown-Leger (2004), Collapse and rapid resumption of Atlantic meridional circulation linked to deglacial climate changes, *Nature*, *428*, 834–837, doi:10.1038/nature02494.

Menviel, L., A. Timmermann, O. E. Timm, and A. Mouchet (2011), Deconstructing the Last Glacial Termination: The role of millennial and orbital-scale forcings, *Quat. Sci. Rev.*, *30*, 1155–1172, doi:10.1016/j.quascirev.2011.02.005.

Menviel, L., A. Timmermann, O. E. Timm, A. Mouchet, A. Abe-Ouchi, M. Chikamoto, N. Harada, R. Ohgaito, and Y. Okazaki (2012), Removing the North Pacific halocline: Effects on global climate, ocean circulation and the carbon cycle, *Deep Sea Res. Part II*, *61*, 106–113, doi:10.1016/j.dsr2.2011.03.005.

Menviel, L., M. England, K. Meissner, A. Mouchet, and J. Yu (2014), Atlantic-Pacific seesaw and its role in outgassing CO_2 during Heinrich events, *Paleoceanography*, *29*, 58–70, doi:10.1002/2013PA002542.

Okazaki, Y., A. Timmermann, L. Menviel, N. Harada, A. Abe-Ouchi, M. Chikamoto, A. Mouchet, and H. Asahi (2010), Deepwater formation in the North Pacific during the Last Glacial Termination, *Science*, *329*, 200–204, doi:10.1126/science.1190612.

Okumura, Y. M., C. Deser, A. Hu, A. Timmermann, and S.-P. Xie (2009), North Pacific climate response to freshwater forcing in the subarctic North Atlantic: Oceanic and atmospheric pathways, *J. Clim.*, *22*, 1424–1445, doi:10.1175/2008JCLI2511.1.

Parés, J., N. Hassold, D. Rea, and B. van Der Pluijm (2007), Paleocurrent directions from paleomagnetic reorientation of magnetic fabrics in deep-sea sediments at the Antarctic Peninsula Pacific margin (ODP Sites 1095, 1101), *Mar. Geol.*, *242*, 261–269, doi:10.1016/j.margeo.2007.04.002.

Park, C.-K., S.-J. Doh, D.-W. Suk, and K.-H. Kim (2000), Sedimentary fabric on deep-sea sediments from KODOS area in the eastern Pacific, *Mar. Geol.*, *171*(1), 115–126, doi:10.1016/S0025-3227(00)00107-9.

Pelejero, C., M. Kienast, L. Wang, and J. O. Grimalt (1999), The flooding of Sundaland during the last deglaciation: Imprints in hemipelagic sediments from the southern South China Sea, *Earth Planet. Sci. Lett.*, *171*(4), 661–671, doi:10.1016/S0012-821X(99)00178-8.

Qu, T., J. B. Girton, and J. A. Whitehead (2006), Deepwater overflow through Luzon Strait, *J Geophys Res: Oceans* (*1978–2012*), *111*(C1), doi:10.1029/2005JC003139.

Qu, T., Y. T. Song, and T. Yamagata (2009), An introduction to the South China Sea throughflow: Its dynamics, variability, and application for climate, *Dyn. Atmos. Oceans*, *47*, 3–14, doi:10.1016/j.dynatmoce.2008.05.001.

Rae, J. W., M. Sarnthein, G. L. Foster, A. Ridgwell, P. M. Grootes, and T. Elliott (2014), Deep water formation in the North Pacific and deglacial CO_2 rise, *Paleoceanography*, doi:10.1002/2013PA002570.

Saenko, O. A., A. Schmittner, and A. J. Weaver (2004), The Atlantic-Pacific seesaw, *J. Climate*, *17*, 2033–2038, doi:10.1175/1520-0442(2004)017<2033:TAS>2.0.CO;2.

Shao, L., X. Li, J. Geng, X. Pang, Y. Lei, P. Qiao, L. Wang, and H. Wang (2007), Deep water bottom current deposition in the northern South China Sea, *Sci. China, Ser. D Earth Sci.*, *50*, 1060–1066, doi:10.1007/s11430-007-0015-y.

Shu, Y., H. Xue, D. Wang, F. Chai, Q. Xie, J. Yao, and J. Xiao (2014), Meridional overturning circulation in the South China Sea envisioned from the high-resolution global reanalysis data GLBa0.08, *J. Geophys. Res. Oceans*, *119*, 3012–3028, doi:10.1002/2013JC009583.

Siddall, M., E. J. Rohling, A. Almogi-Labin, C. Hemleben, D. Meischner, I. Schmelzer, and D. Smeed (2003), Sea-level fluctuations during the last glacial cycle, *Nature*, *423*(6942), 853–858, doi:10.1038/nature01690.

Stommel, H. (1961), Thermohaline convection with two stable regimes of flow, *Tellus*, *13*(2), 224–230, doi:10.1111/j.2153-3490.1961.tb00079.x.

Sun, Y., D. W. Oppo, R. Xiang, W. Liu, and S. Gao (2005), Last deglaciation in the Okinawa Trough: Subtropical northwest Pacific link to Northern Hemisphere and tropical climate, *Paleoceanography*, *20*, doi:10.1029/2004PA001061.

Stanford, J., E. Rohling, S. Bacon, A. Roberts, F. Grousset, and M. Bolshaw (2011), A new concept for the paleoceanographic evolution of Heinrich event 1 in the North Atlantic, *Quat. Sci. Rev.*, *30*(9), 1047–1066, doi:10.1016/j.quascirev.2011.02.003.

Talley, L. D., J. L. Reid, and P. E. Robbins (2003), Data-based meridional overturning streamfunctions for the global ocean, *J. Clim.*, *16*(19), 3213–3226, doi:10.1175/1520-0442(2003)016<3213:DMOSFT>2.0.CO;2.

Wan, S., and Z. Jian (2014), Deep water exchanges between the South China Sea and the Pacific since the Last Glacial Period, *Paleoceanography*, doi:10.1002/2013PA002578.

Wan, S., A. Li, P. D. Clift, S. Wu, K. Xu, and T. Li (2010), Increased contribution of terrigenous supply from Taiwan to the northern South China Sea since 3 Ma, *Mar. Geol.*, *278*(1), 115–121, doi:10.1016/j.margeo.2010.09.008.

Wang, G., S. P. Xie, T. Qu, and R. X. Huang (2011), Deep South China Sea circulation, *Geophys. Res. Lett.*, *38*, doi:10.1029/2010GL046626.

Wei, G.-J., C.-Y. Huang, C.-C. Wang, M.-Y. Lee, and K.-Y. Wei (2006), High-resolution benthic foraminifer $\delta^{13}C$ records in the South China Sea during the last 150 ka, *Mar. Geol.*, *232*(3), 227–235, doi:10.1016/j.margeo.2006.08.005.

Wolff, J. A., B. B. Ellwood, and S. D. Sachs (1989), Anisotropy of magnetic susceptibility in welded tuffs: Application to a welded-tuff dyke in the Tertiary Trans-Pecos Texas volcanic province, USA, *Bull. Volcanol.*, *51*(4), 299–310.

Wu, Q., C. Colin, Z. Liu, F. Thil, Q. Dubois-Dauphin, N. Frank, K. Tachikawa, L. Bordier, and E. Douville (2015), Neodymium isotopic composition in foraminifera and authigenic phases of South China Sea sediments: Implications for the hydrology of the North Pacific Ocean over the past 25 kyr, *Geochem. Geophys. Geosyst.*, doi:10.1002/2015GC005871.

Wu, Y., Z. Zhu, S. Qiu, Y. Han, J. Cai, and Z. Rao (2016), Magnetic stratigraphy constraints on the Matuyama–Brunhes boundary recorded in a loess section at the southern margin of Chinese Loess Plateau, *Geophys. J. Int.*, *204*, 1072–1085, doi:10.1093/gji/ggv502.

Yu, K., Q. Hua, J. X. Zhao, E. Hodge, D. Fink, and M. Barbetti (2010), Holocene marine ^{14}C reservoir age variability: Evidence from ^{230}Th-dated corals in the South China Sea, *Paleoceanography*, *25*, doi:10.1029/2009PA001831.

Zhao, Y., Z. Liu, Y. Zhang, J. Li, M. Wang, W. Wang, and J. Xu (2015), In situ observation of contour currents in the northern South China Sea: Applications for deepwater sediment transport, *Earth Planet. Sci. Lett.*, *430*, 477–485, doi:10.1016/j.epsl.2015.09.008.s.